3D study of intermetallics and their effect on the corrosion morphology of rheocast aluminium alloy

CrossMark

B. Mingo [a], R. Arrabal [a,*], A. Pardo [a], E. Matykina [a], P. Skeldon [b]

[a] Departamento de Ciencia de Materiales, Facultad de Ciencias Químicas, Universidad Complutense, 28040, Madrid, Spain
[b] Corrosion and Protection Group, School of Materials, The University of Manchester, Manchester M13 9PL, UK

ABSTRACT

In the present study, the effect of heat treatment T6.1 on the microstructure and corrosion behaviour of rheocast aluminium alloy A356 is investigated on the basis of 2D/3D characterization techniques and electrochemical and SKPFM measurements. Heat treatment strengthens the α-Al matrix, modifies the intermetallic particles and spheroidizes eutectic Si. These changes do not modify significantly the corrosion behaviour of the alloy.
3D SEM-Tomography clearly shows that the corrosion advances in the shape of narrow paths between closely spaced intermetallics without a major influence of eutectic Si.

© 2015 Elsevier Inc. All rights reserved.

1. Introduction

The growing demand for high performance light materials in the automotive industry has triggered the development of new processing routes. Semisolid metal (SSM) processing is expected to substitute traditional casting processes due to the possibility of producing heat treatable, defect-free and near-net shape components at lower prices [1]. The success of SSM processing lies in the possibility of handling the material in the semisolid state, where it presents thixotropic properties which allows the filling of the mould under laminar flow conditions avoiding gas entrapment. This results in materials with homogeneous globular microstructures with reduced porosity and segregation [2].

Most semisolid processes are derived from two major techniques: rheocasting and thixocasting. During rheocasting the alloy is kept in the semisolid state under continuous agitation before injecting or pouring into the die; while thixocasting involves the partial remelting of the billet into the semisolid region [3].

Al–Si alloys stand out for their excellent castability, good corrosion behaviour in most media and favorable mechanical properties such as impact strength and crack propagation resistance [4], which are highly desired in the manufacturing of vehicles. However, specific parts of the vehicles that are subjected to hostile environments are required to

have even better mechanical performance [5], which could be achieved by using SSM processing and/or heat treatments [6].

Heat treatments improve the strength of aluminum alloys through precipitation-hardening processes that take place as a consequence of changes in the solubility of alloying elements in the matrix with temperature [7]. Al–Si alloys are usually alloyed with Mg since it reacts with Si forming sub-micrometre Mg_2Si precipitates which are responsible of the hardening of the alloy [7,8]. Magnesium also promotes the precipitation of Al–Fe–Si–Mg compounds, which improve the tensile strength, yield strength and hardness compared with magnesium-free alloys [9].

Although mechanical properties of heat-treated cast and semisolid Al-Si alloys have been deeply investigated [10,11], there are very few studies about their corrosion performance. For instance, Sheng-Long Lee et al. [12] studied an as-cast Al7Si0.3Mg alloy and observed a positive effect of T4, T6 and T7 heat treatments on the corrosion resistance, which was associated with the spheroidization and coarsening of eutectic Si. Osorio [13] and Bastidas [14] also attributed the slight improvement of the corrosion performance of heat-treated as-cast Al–9 wt.% Si and rheocast A357 aluminium alloys to the eutectic silicon modification. However, very little attention has been given to the role of intermetallic particles. Previous studies by the authors on rheocast and gravity-cast A356 alloy demonstrated that corrosion initiates at the interface between the α-Al matrix and the Fe-rich intermetallics as a result of microgalvanic corrosion processes. These locations correspond to pit nucleation sites which then grow, progressing through the regions

* Corresponding author.
  E-mail address: rarrabal@ucm.es (R. Arrabal).

surrounding the eutectic silicon [2]. Therefore, it was presumed that intermetallic particles were only detrimental at the initial stages of corrosion.

The previous studies have evaluated the corrosion progress from longitudinal and cross-section examination, which limits the analysis of the real evolution of corrosion in the bulk material. With the recent development of 3-dimensional (3D) characterization techniques, such as 3D SEM-tomography, it is possible to gain further knowledge on the corrosion morphology, corrosion mechanism and role of secondary phases interfaces [15–18].

The aim of this study is to evaluate in 3D the corrosion progression in a commonly used Al–Si alloy (A356) produced by a rheocast procedure and the effect of T6.1 heat treatment. Special attention is given to the participation of intermetallic particles in the corrosion process.

2. Material and methods

2.1. Test materials

Rheocast aluminium alloy, A356-RC, was obtained by heating a commercial alloy up to 720 °C in a metallic vessel (Ø = 35 mm), cooling down to the semisolid region (580 °C) under continuous electromagnetic agitation, and finally quenching in cold water. The chemical composition of the alloy is 6.72Si, 0.155Fe, 0.0006Mn, 0.369Mg, 0.156Ti, 0.001Zn, 0.015Sr, bal. Al (wt.%). 2 mm-thick samples were subjected to T6.1 treatment which consisted of a solution treatment at 540 °C for 2 h, water quenching, natural aging for 12 h and artificial aging at 155 °C for 2 h. The latter time was selected in order to obtain the highest hardness (Fig. 1).

2.2. Specimen preparation and characterization

2D metallographic characterization of studied alloys was performed on longitudinal specimens which were wet-ground through successive grades of SiC abrasive paper and polished to 0.1 μm diamond finish. Microconstituents were revealed by using the Weck reagent (4 g $KMnO_4$, 1 g NaOH, 200 mL H_2O). The specimens were examined by optical microscopy (Leica-Reichert MEF4 A/M) and by scanning electron microscopy (SEM, JEOL JSM-6400 equipped with Oxford Link energy dispersive X-ray microanalysis hardware). The alloy hardness was evaluated using an AVK-AΠ Vickers hardness tester on ground specimens under a load of 5 kg for 20 s. The cited values are the average of ten measurements. Second phase particles were characterized by transmission electron microscopy (TEM JEOL 2000-FX, operated at 200 kV). TEM samples (disks with a diameter of 3 mm and 100 μm-thick) were

prepared by ion milling using a Gatan PIPS system with a small incident angle until perforation. Quantitative metallography studies were performed using ImageJ software, analyzing five SEM micrographs for each specimen.

A Nanoscope IIIa MultiMode scanning Kelvin probe force microscope (SKPFM, Veeco-Digital Instruments) equipped with a silicon tip coated with platinum (20 nm thickness) was used to measure surface potential maps of polished specimens (0.1 μm diamond finish). A reference sample of aluminium coated with a thin gold layer was used for calibration of the tip. Topographic and surface potential images were taken simultaneously working in tapping mode using a two-pass technique, keeping a constant sample distance of 100 nm. The height profile was recorded during the first scan and the potential profile was acquired during the second scan. The measurements were made at relative humidity of 30–40% and room temperature.

3D characterization specimens were prepared by grinding the specimens in the shape of a truncated pyramid, placing the surface of interest at the top surface of the pyramid. Then, the samples were trimmed with a glass knife in a ultramicrotome (Leica Ultracut), followed by final cutting with a diamond knife. Sequential backscattered SEM micrographs were taken in a Quanta 250 FEG-SEM equipped with an in-situ ultramicrotome (Gatan 3View and XuM) at low voltages (~2.5 kV), which provide enhanced depth and lateral resolution [15,18]. The volumetric reconstruction was performed using the Avizo Fire 6.3 software.

2.3. Corrosion tests

A computer controlled AUTOLAB potentiostat (PGSTAT 30) and a three-electrode cell were used to perform the electrochemical measurements. A graphite electrode was used as the counter electrode and silver/silver chloride (Ag/AgCl in 3 M KCl) was used as the reference electrode. The working area of the material was 1 cm^2. Cyclic polarization curves were obtained after 24 h of immersion in naturally-aerated 3.5 wt.% NaCl solution (22 °C, pH 6.5) using a scanning rate of 0.3 mV/s, starting from −150 mV vs. the open circuit potential (OCP) and limiting the current to 5 mA/cm^2.

The early stages of corrosion were evaluated after immersion of specimens in naturally-aerated NaCl 3.5 wt.% solution for 6 h by using 3D SEM-tomography. Specimens were prepared similarly to those described in Section 2.2.

3. Results and discussion

3.1. Microstructure of the alloys

A356-RC aluminium alloy (84 ± 4 HV$_5$) has the characteristic microstructure of semisolid alloys comprising a globular α-Al matrix (shape factor 6.70 ± 0.04) and fibrous/globular eutectic Si located at the interglobular regions (Fig. 2a). Quantitative and morphological information of the phases present in the studied materials is collected in Table 1. Fe impurities in Al–Si commercial alloys result in the formation of Fe-rich intermetallic compounds, since the solubility of Fe in Al is very low [19]. In the case of the A356-RC alloy, SEM/EDS/TEM studies revealed three types of intermetallics localized at the interglobular regions: β-Al$_5$FeSi, π-AlFeSiMg and Mg$_2$Si. The β-Al$_5$FeSi intermetallic acts as stress raiser increasing the brittleness of the alloy [20]. In 2D characterization this phase resembles needles [2], but in a 3D rendered tomographic volume a platelet morphology is clearly observed (Fig. 2b, Video 1). π-AlFeSiMg (π-Al$_{8.64}$FeSi$_5$–Mg$_{3.36}$) and Mg$_2$Si intermetallic compounds are formed as a consequence of the presence of Mg in the alloy and precipitate as inclusions between the Si plates and the eutectic Al matrix. They present Chinese script and globular morphologies respectively, which are less detrimental from a mechanical point of view. Fig. 2c and Video 2 show the 3D micrograph of π-AlFeSiMg, where the hole-shaped and highly interconnected morphology of this phase can be observed.
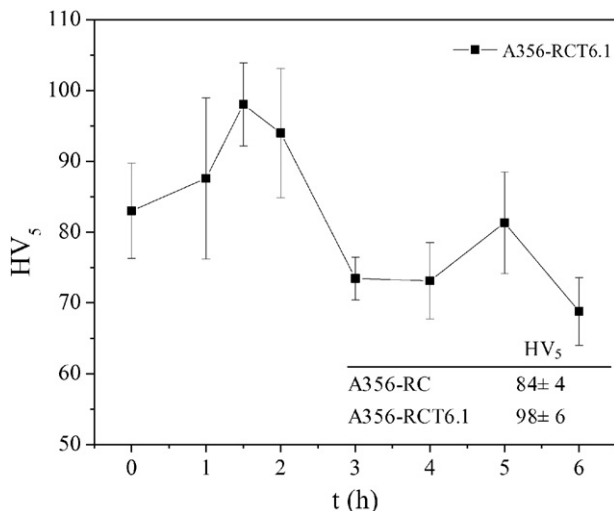

Fig. 1. Vickers hardness as a function of the solution treatment time.